

## Exploring Excited Hadrons

---

**Colin Morningstar\***

*Department of Physics, Carnegie Mellon University, Pittsburgh, PA 15213, USA*

*E-mail: colin\_morningstar@cmu.edu*

Progress in extracting the spectrum of excited hadron resonances is reviewed and the key issues and challenges in such computations are outlined. The importance of multi-hadron states as simulations are done with lighter pion masses is discussed, and the need for all-to-all quark propagators is emphasized.

*The XXVI International Symposium on Lattice Field Theory*

*July 14 - 19, 2008*

*Williamsburg, Virginia, USA*

---

\*Speaker.

## 1. Introduction

Experiments show that many excited-state hadrons exist, and there are significant experimental efforts to map out the QCD resonance spectrum, such as Hall B and the proposed Hall D at Jefferson Lab, ELSA associated with the University of Bonn, COMPASS at CERN, PANDA at GSI, and BESIII in Beijing. Hence, there is a great need for *ab initio* determinations of such states in lattice QCD.

Higher-lying excited hadrons are a new frontier in lattice QCD, and explorations of new frontiers are usually fraught with dangers. Excited states are more difficult to extract in Monte Carlo calculations; correlation matrices are needed and operators with very good overlaps onto the states of interest are crucial. To study a particular state of interest, all states lying below that state must first be extracted, and as the pion gets lighter in lattice QCD simulations, more and more multi-hadron states will lie below the excited resonances. To reliably extract these multi-hadron states, multi-hadron operators made from constituent hadron operators with well-defined relative momenta will most likely be needed, and the computation of temporal correlation functions involving such operators will require the use of all-to-all quark propagators. The evaluation of disconnected diagrams will ultimately be required. Perhaps most worrisome, most excited hadrons are unstable (resonances), so the results obtained for finite-box stationary-state energies must be interpreted carefully.

This talk will describe the key issues and challenges in exploring excited hadrons in lattice QCD, emphasizing the importance of multi-hadron operators and the need for all-to-all quark propagators. Dealing with resonances in a box is discussed, and the technology associated with extracting excited stationary-state energies, including operator design and field smearing, is detailed. Efforts in variance reduction of stochastically-estimated all-to-all quark propagators using source dilutions are outlined. Results on excited hadrons during the last year are summarized.

## 2. Resonances in a box

A simple example serves to illustrate the issues that must be confronted when studying resonances in a box. Consider the (dimensionless) Hamiltonian for a single nonrelativistic particle of mass  $m = 1$  moving in one dimension in a potential  $V(x)$  is given by

$$H = \frac{1}{2}p^2 + V(x), \quad V(x) = (x^4 - 3) e^{-x^2/2}. \quad (2.1)$$

This potential has an attractive core surrounded by a repulsive barrier, as shown in Fig. 1. The infinite-volume spectrum of this Hamiltonian for energies  $E < 4$  is shown in Fig. 1. The ground state is a bound state of even parity, and there is one bound state in the odd parity channel. A continuum of scattering states is found for  $E > 0$ , with a narrow resonance in the even-parity channel and a broad resonance in the odd-parity sector, both below 4. Even (+) and odd (−) parity scattering phase shifts  $\delta_{\pm}(E)$  can be defined in the usual way as the phase between the transmitted and incident wave, appearing in the asymptotic wave functions as

$$\varphi_k^{(+)}(x) = c_+ \cos\left(k|x| + \delta_+(k)\right), \quad \varphi_k^{(-)}(x) = c_- \operatorname{sgn}(x) \sin\left(k|x| + \delta_-(k)\right), \quad (|x| \rightarrow \infty), \quad (2.2)$$

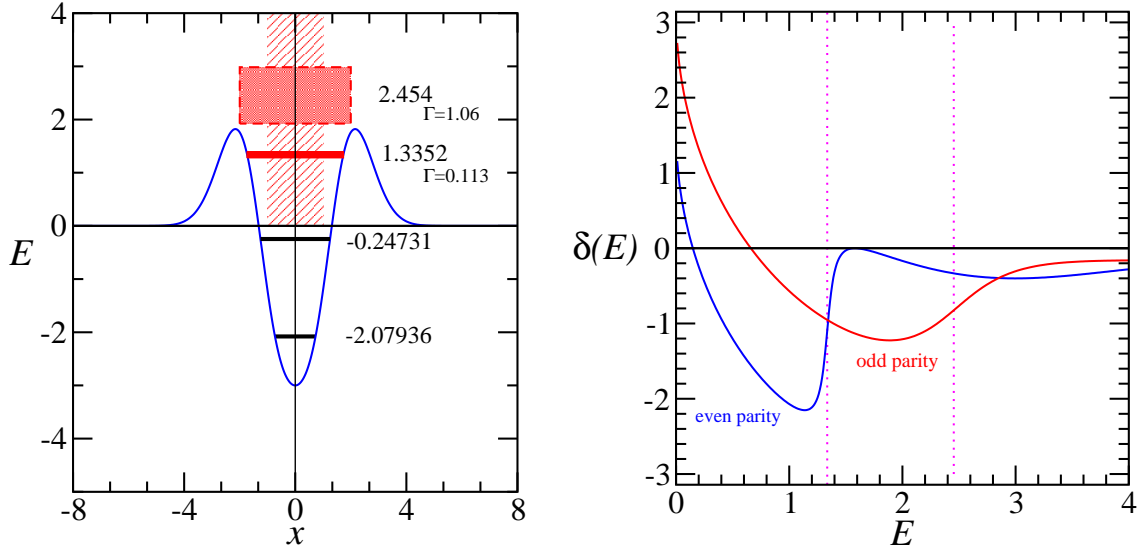


**Figure 1:** (Left) The solid curve shows the potential  $V(x)$  of the example given in Eq. (2.1). The spectrum for energies  $E < 4$  is also shown. The ground state is an even-parity bound state, and there is one bound state in the odd-parity channel. Two resonances (a narrow one in the even-parity and a very broad one in the odd parity sector) in a continuum of scattering states  $E > 0$  are shown. (Right) The scattering phases  $\delta_{\pm}(E)$  for this example are shown for  $E < 4$ . The locations of the resonance energies are shown as dashed vertical lines.

where  $k = \sqrt{2E}$ . These phase shifts are also shown in Fig. 1. The narrow even-parity resonance is seen as a sudden dramatic increase in the phase shift (by an amount comparable to  $\pi$ ) and the broad odd-parity resonance appears as a not-so-sudden increase in the phase shift. The resonance masses and widths can be extracted by fitting a Breit-Wigner plus a polynomial background to  $d\delta_{\pm}/dE$  in the vicinity of the resonances (or by employing the complex rotation method described in Ref. [1]).

Now consider solving the system in a box of length  $L$  such that  $-\frac{1}{2}L < x < \frac{1}{2}L$ , assuming periodic boundary conditions. Note that the potential is now  $V_L(x) = \sum_{n=-\infty}^{\infty} V(x+nL)$ . The infinite volume gets tiled into  $L$ -length strips in which the potential is replicated. We assume that  $L$  is large compared to the extent of the potential  $V$  so that interactions with mirror potentials is negligible.

In a finite-box with periodic boundary conditions, the momentum is quantized, so the entire spectrum is a series of discrete energies, even for  $E > 0$ . The periodic-box spectrum can be determined in two ways: diagonalization of the Hamiltonian in a basis of states having appropriate boundary conditions, and by solving the differential equation and matching to an asymptotic form having the correct boundary conditions. Either way, one finds the spectrum shown in Fig. 2. The light dotted lines indicate the spectrum for  $V = 0$  which have values  $2\pi^2 n^2/L^2$  for  $n = 1, 2, 3, \dots$ , plus an  $n = 0$  line in the even parity channel. One sees that a resonance shows up as a series of avoided level crossings when viewed against box length  $L$ . A narrow resonance, as in the even parity sector, can be easily identified by a closely-avoided level crossing, but a broad resonance, as in the odd parity sector, is essentially impossible to recognize.

These plots illustrate the difficulty in extracting resonance parameters from finite-box energies. Under certain special circumstances, resonance parameters can be ferreted out using tricks such as

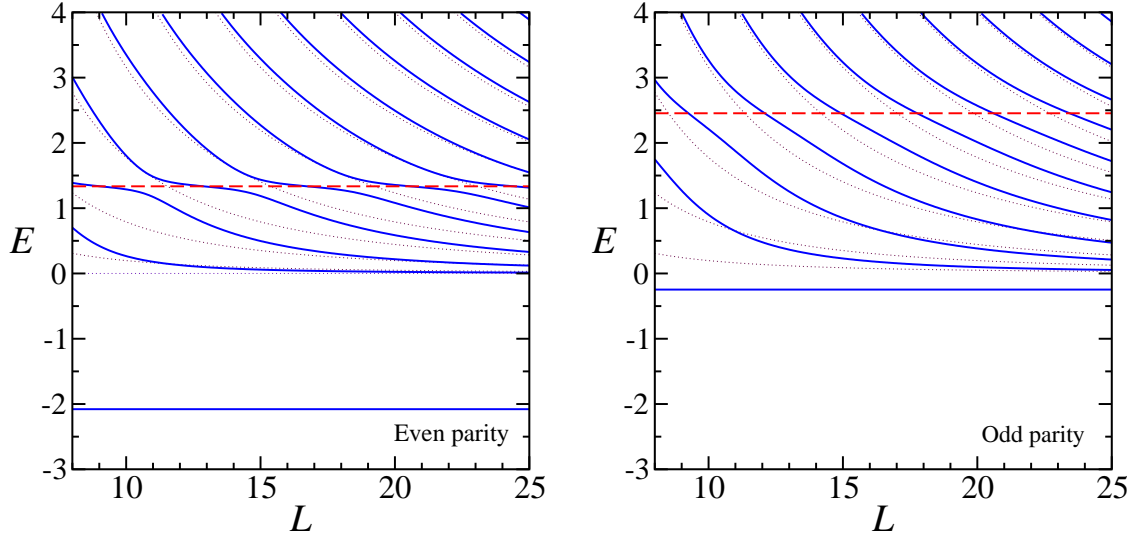


**Figure 2:** (Left) Spectrum of even-parity states for the example Hamiltonian given in Eq. (2.1) in a box of extent  $L$  with periodic boundary conditions. (Right) Spectrum of odd-parity states. The light dotted lines indicate the energy levels for  $V = 0$  which have values  $2\pi^2 n^2 / L^2$  for  $n = 1, 2, 3, \dots$ , plus an  $n = 0$  line in the even parity channel. The horizontal dashed lines show the locations of the infinite-volume resonance energies.

described in Ref. [2]. Examining the spectrum in several volumes is important, and knowing the pattern of multi-hadron states based on mass determinations of the stable particles and group-theoretical combinations of the constituents having total zero-momentum certainly helps. For high precision, the phase-shift method of Refs. [3, 4] can be used. In this method, the finite-volume energies are used to determine the scattering phase shifts of the partial waves, from which one can deduce resonance masses and widths. This method has recently been applied to study the  $\rho$ -meson resonance[5]. The  $\pi\pi$  phase shift was extracted from the finite-volume spectrum, and the

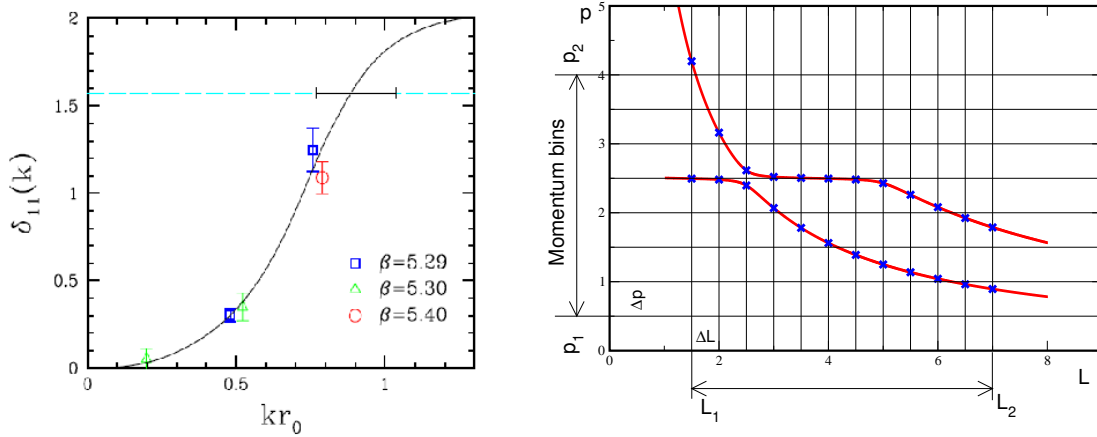


**Figure 3:** (Left)  $\pi\pi$  scattering phase shift showing the  $\rho$ -resonance [5]. A width  $\Gamma_\rho = 200^{+130}_{-100}$  MeV is obtained from a Breit-Wigner fit. (Right) Illustration of the binning method of Ref. [6] in which a probability distribution is used to identify resonant structure. For various values of  $L$ , energies are collected into momentum bins to construct a probability distribution  $W(p)$ .

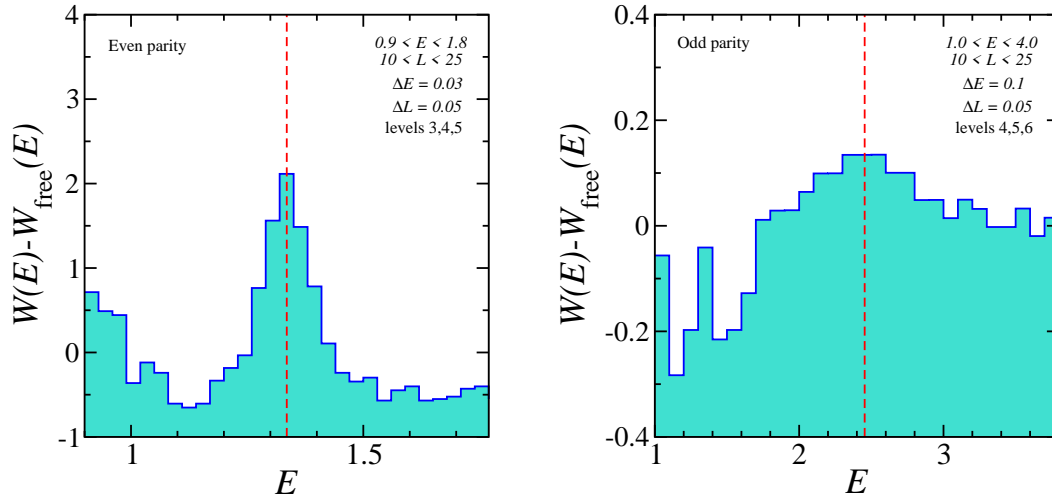


**Figure 4:** (Left) Results of applying the binning method of Ref. [6] near the even-parity resonance of the example Hamiltonian in Eq. (2.1). Location of the resonance is indicated by the vertical dashed line. (Right) Results for the very broad odd-parity resonance.

$\rho$  resonance parameters extracted (see Fig. 3). However, the practicality of the phase-shift method has yet to be demonstrated for other resonances in QCD.

A new histogram method has been recently proposed[6] and applied to synthetic pion-nucleon data which mocks up the  $\Delta$ -resonance. Energies for several volumes are collected into momentum bins, and with suitable normalization and free-result subtraction, such histograms produce a probability distribution  $W(p)$  which shows peaks corresponding to the resonances of interest (see Fig. 3). The method has no prior theoretical bias and provides the possibility of seeing resonant structure even when avoided level crossings are washed out by a broad resonance. The application of this method to the example Hamiltonian in Eq. (2.1) is shown in Fig. 4. The narrow resonance appears quite clearly, and amazingly, the odd-parity broad resonance is also correctly reproduced.

Deducing resonance parameters from finite-box spectra remains a difficult challenge, especially considering that higher-lying resonances will lie above three-particle and four-particle thresholds and that these resonances can have multiple decay channels. Certainly, further work in this area is needed. Perhaps matching the finite-box spectra to that of an effective theory, such as a one-boson exchange model, might ultimately be the way to make progress.

### 3. Excited stationary states: recent results

Before discussing the issues and challenges in extracting the energies of stationary states in a box, I would like to summarize the excited-state results which have appeared since the last lattice conference.

A first glimpse of the higher-lying nucleon spectrum in lattice QCD was provided by the Hadron Spectrum Collaboration in Ref. [7]. These first results, shown in Fig. 5, were on a small  $12^3 \times 48$  anisotropic quenched lattice with a very heavy pion. Results for both the nucleons and  $\Delta$ -resonances on 239 quenched configurations on a  $16^3 \times 64$  lattice and 167 quenched configura-

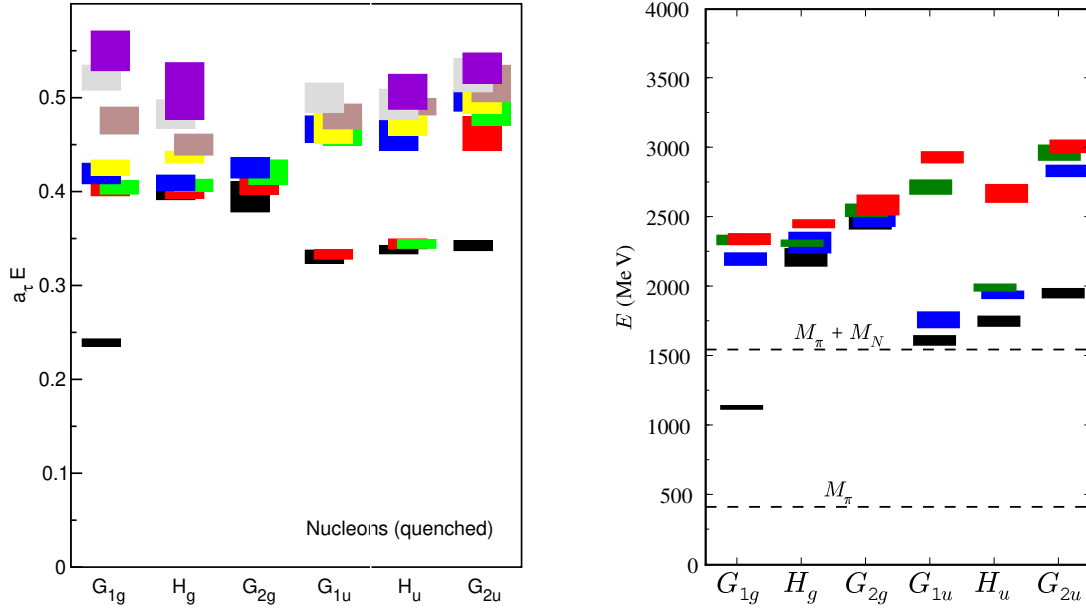


**Figure 5:** (Left) Nucleon spectrum from 200 quenched configurations on a  $12^3 \times 48$  anisotropic lattice using the Wilson gauge and quark actions with  $a_s \sim 0.1$  fm,  $a_s/a_t \sim 3.0$  and  $m_\pi \sim 700$  MeV from Ref. [7]. (Right) Nucleon spectrum from 430  $N_f = 2$  configurations on a  $24^3 \times 64$  lattice using a stout-smearred clover fermion action and Symanzik-improved gauge action with  $a_s \sim 0.1$  fm,  $a_s/a_t \sim 3$ , and  $m_\pi = 400$  MeV from Ref. [9].

tions on a  $24^3 \times 64$  lattice using an anisotropic Wilson action with spatial spacing  $a_s \sim 0.1$  fm,  $a_s/a_t \sim 3$ , and a pion mass  $m_\pi \sim 490$  MeV appeared during the past year[8]. These masses have been determined in the past year using 430  $N_f = 2$  configurations on a  $24^3 \times 64$  lattice with a stout-smearred clover fermion action and a Symanzik-improved anisotropic gauge action[9]. The results for a pion mass  $m_\pi = 400$  MeV, spacing  $a_s \sim 0.1$  fm and  $a_s/a_t \sim 3$  are shown in Fig. 5. The low-lying odd-parity band shows the exact number of states in each channel as expected from experiment. The two figures show the splittings in the band increasing as the quark mass is decreased. At these heavy pion masses, the first excited state in the  $G_{1g}$  channel is significantly higher than the experimentally measured Roper resonance. It remains to be seen whether or not this level will drop down as the pion mass is further decreased. Most of the levels in the right-hand plot lie very close to two-particle thresholds. The use of two-hadron operators will be needed to go to lighter pion masses.

During the past year, extractions of excited meson states have been presented in Ref. [10]. Results in the pseudoscalar, vector, and axial-vector channels are shown in Fig. 6. These results were obtained using 99 quenched configurations on a  $16^3 \times 32$  isotropic lattice with a chirally-improved fermion action and the Luscher-Weisz gauge action for lattice spacing  $a_s \sim 0.15$  fm and a range of pion masses. This work emphasizes the use of derivative sources in correlation matrices to obtain the excited states. A search for light scalar tetraquark states with isospin  $I = 0, \frac{1}{2}$  was also presented at this conference[11].

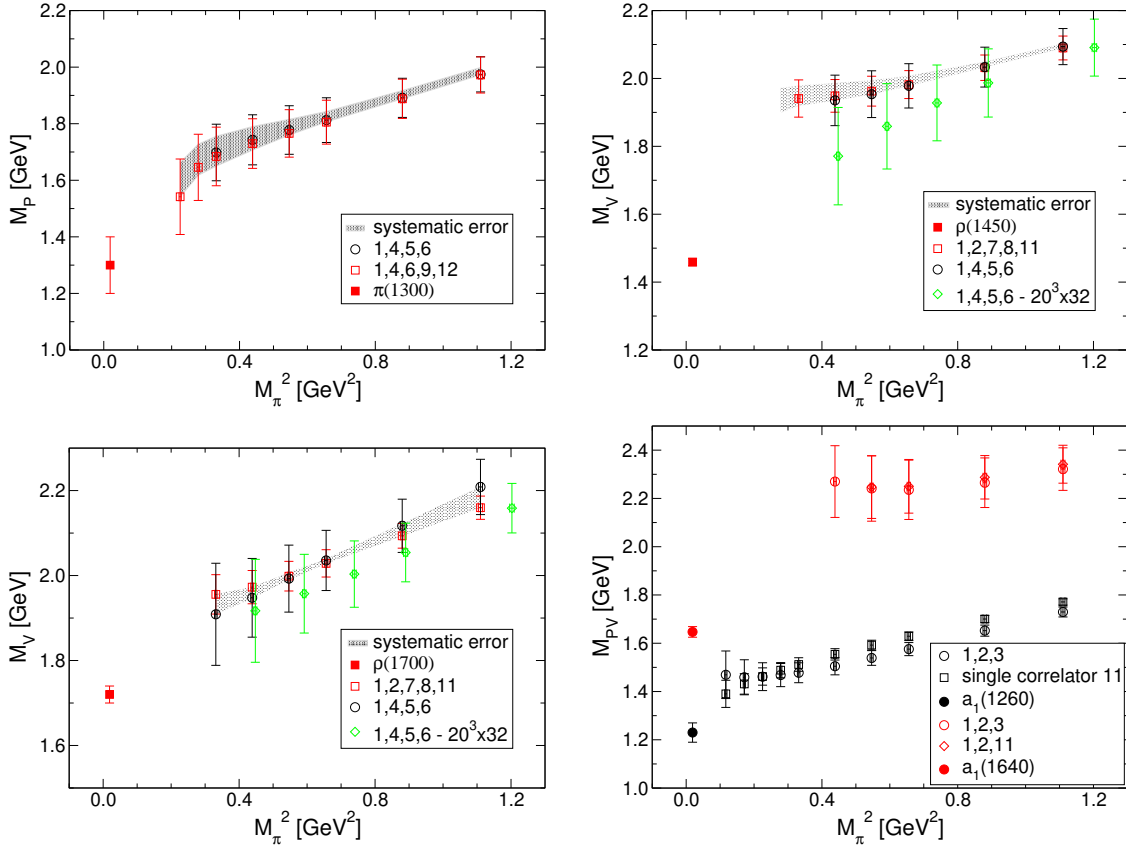


**Figure 6:** (Upper left) Results from Ref. [10] for the first-excited pseudoscalar  $0^{-+}$  meson mass against pion mass squared from 99 quenched configurations on a  $16^3 \times 32$  lattice with a chirally-improved fermion action and the Luscher-Weisz gauge action for lattice spacing  $a_s \sim 0.15$  fm. (Upper right) First-excited  $1^{--}$  meson mass. (Lower left) Second-excited  $1^{--}$  meson mass. (Lower right) Ground and first-excited  $1^{++}$  meson masses.

#### 4. Excited stationary states: key issues

Reliably capturing the masses of excited states requires the computation of correlation matrices  $C_{ij}(t) = \langle 0 | T \Phi_i(t) \Phi_j^\dagger(0) | 0 \rangle$  associated with a large set of  $N$  different operators  $\Phi_i(t)$ . It has been shown in Ref. [12] that the  $N$  principal effective masses  $W_\alpha(t)$ , defined by

$$W_\alpha(t) = \ln \left( \frac{\lambda_\alpha(t, t_0)}{\lambda_\alpha(t+1, t_0)} \right),$$

where  $\lambda_\alpha(t, t_0)$  are the eigenvalues of  $C(t_0)^{-1/2} C(t) C(t_0)^{-1/2}$  and  $t_0 < t/2$  is usually chosen, tend to the eigenenergies of the lowest  $N$  states with which the  $N$  operators overlap as  $t$  becomes large. The eigenvectors associated with  $\lambda_\alpha(t, t_0)$  can be viewed as variationally optimized operators. When combined with appropriate fitting and analysis methods, such variational techniques are a particularly powerful tool for investigating excitation spectra. To extract the stationary state energies, one can fit a single-exponential or a sum of two exponentials to each principal correlator; alternatively, optimized operators can be determined on an early time slice, and a fit to the

correlation matrix of optimized operators can be carried out. The use of both methods is a good consistency check.

The use of operators whose correlation functions  $C(t)$  attain their asymptotic form as quickly as possible is crucial for reliably extracting excited hadron masses. An important ingredient in constructing such hadron operators is the use of smeared fields. Operators constructed from smeared fields have dramatically reduced mixings with the high frequency modes of the theory. Both link-smearing and quark-field smearing should be applied. Since excited hadrons are expected to be large objects, the use of spatially extended operators is another key ingredient in the operator design and implementation. A more detailed discussion of these issues can be found in Ref. [13].

Spatial links can be smeared using the stout-link procedure described in Ref. [14]. The stout-link smearing scheme is analytic, efficient, and produces smeared links which are automatically elements of  $SU(3)$  without the need for a projection back into  $SU(3)$ . Note that only spatial staples are used in the link smoothening; no temporal staples are used, and the temporal link variables are not smeared. The smeared quark fields can be defined by

$$\tilde{\psi}(x) = \left(1 + \frac{\sigma_s^2}{4n_\sigma} \tilde{\Delta}\right)^{n_\sigma} \psi(x), \quad (4.1)$$

where  $\sigma_s$  and  $n_\sigma$  are tunable parameters ( $n_\sigma$  is a positive integer) and the three-dimensional covariant Laplacian operators are defined in terms of the smeared link variables  $\tilde{U}_j(x)$  as follows:

$$\tilde{\Delta}O(x) = \sum_{k=\pm 1, \pm 2, \pm 3} \left( \tilde{U}_k(x)O(x+\hat{k}) - O(x) \right), \quad (4.2)$$

where  $O(x)$  is an operator defined at lattice site  $x$  with appropriate color structure, and noting that  $\tilde{U}_{-k}(x) = \tilde{U}_k^\dagger(x-\hat{k})$ . The smeared fields  $\tilde{\psi}$  and  $\tilde{\bar{\psi}}$  are Grassmann-valued; in particular, these fields anticommute in the same way that the original fields do, and the square of each smeared field vanishes.

Hadron states are identified by their momentum  $\mathbf{p}$ , intrinsic spin  $J$ , projection  $\lambda$  of this spin onto some axis, parity  $P = \pm 1$ , and quark flavor content (isospin, strangeness, *etc.*). Some mesons also include  $G$ -parity as an identifying quantum number. If one is interested only in the masses of these states, one can restrict attention to the  $\mathbf{p} = \mathbf{0}$  sector, so operators must be invariant under all spatial translations allowed on a cubic lattice. The little group of all symmetry transformations on a cubic lattice which leave  $\mathbf{p} = \mathbf{0}$  invariant is the octahedral point group  $O_h$ , so operators may be classified using the irreducible representations (irreps) of  $O_h$ . For mesons, there are ten irreducible representations  $A_{1g}, A_{2g}, E_g, T_{1g}, T_{2g}, A_{1u}, A_{2u}, E_u, T_{1u}, T_{2u}$ . The representations with a subscript  $g(u)$  are even (odd) under parity. The  $A$  irreps are one dimensional, the  $E$  irreps are two dimensional, and the  $T$  irreps are three-dimensional. The  $A_1$  irreps contain the  $J = 0, 4, 6, 8, \dots$  states, the  $A_2$  irreps contain the  $J = 3, 6, 7, 9, \dots$  states, the  $E$  irreps contain the  $J = 2, 4, 5, 6, 7, \dots$  states, the  $T_1$  irreps contain the spin  $J = 1, 3, 4, 5, \dots$  mesons, and the  $T_2$  irreps contain the spin  $J = 2, 3, 4, 5, \dots$  states. For baryons, there are four two-dimensional irreps  $G_{1g}, G_{1u}, G_{2g}, G_{2u}$  and two four-dimensional representations  $H_g$  and  $H_u$ . The  $G_1$  irrep contains the  $J = \frac{1}{2}, \frac{7}{2}, \frac{9}{2}, \frac{11}{2}, \dots$  states, the  $H$  irrep contains the  $J = \frac{3}{2}, \frac{5}{2}, \frac{7}{2}, \frac{9}{2}, \dots$  states, and the  $G_2$  irrep contains the  $J = \frac{5}{2}, \frac{7}{2}, \frac{11}{2}, \dots$  states. The continuum-limit spins  $J$  of our states must be deduced by examining degeneracy patterns across the different  $O_h$  irreps.



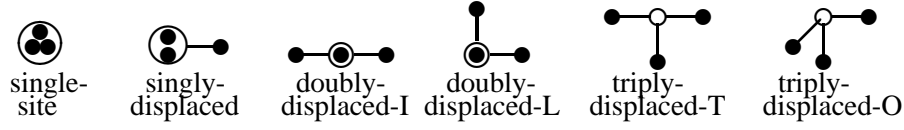


**Figure 7:** The spatial arrangements of the extended three-quark baryon operators. Smeared quark-fields are shown by solid circles, line segments indicate gauge-covariant displacements, and each hollow circle indicates the location of a Levi-Civita color coupling. For simplicity, all displacements have the same length in an operator. Results presented here used displacement lengths of  $3a_s$  ( $\sim 0.3$  fm).

The authors of Ref. [13] advocate operators designed with one eye towards maximizing overlaps with the low-lying states of interest, and the other eye towards minimizing the number of sources needed to calculate the required quark propagators. They emphasize that a construction method which can be easily adapted for baryons, mesons, hybrid states, and multi-hadron systems is ideal. Since the calculation of quark propagators can be computationally expensive, baryon, meson, and multiquark operators which share the same basic building blocks is recommended.

Thus, these authors advocate a three-stage approach to constructing hadron operators. First, basic building blocks are chosen. These are taken to be smeared covariantly-displaced quark fields

$$(\tilde{D}_j^{(p)} \tilde{\Psi})_{a\alpha}^A, (\tilde{\Psi} \tilde{D}_j^{(p)\dagger})_{a\alpha}^A, \quad -3 \leq j \leq 3, \quad (4.3)$$

where  $A$  is a flavor index,  $a$  is a color index,  $\alpha$  is a Dirac spin index, and the  $p$ -link gauge-covariant displacement operator in the  $j$ -th direction is defined by

$$\tilde{D}_j^{(p)}(x, x') = \tilde{U}_j(x) \tilde{U}_j(x+\hat{j}) \dots \tilde{U}_j(x+(p-1)\hat{j}) \delta_{x', x+p\hat{j}}, \quad \tilde{D}_0^{(p)}(x, x') = \delta_{xx'}, \quad (4.4)$$

for  $j = \pm 1, \pm 2, \pm 3$  and  $p \geq 1$ , and where  $j = 0$  defines a zero-displacement operator to indicate no displacement. Next, *elemental* operators  $B_i^F(t, \mathbf{x})$  are devised having the appropriate flavor structure characterized by isospin, strangeness, *etc.*, and color structure constrained by gauge invariance. For zero momentum states, translational invariance is imposed:  $B_i^F(t) = \sum_{\mathbf{x}} B_i^F(t, \mathbf{x})$ . Finally, group-theoretical projections are applied to obtain operators which transform irreducibly under all lattice rotation and reflection symmetries:

$$\mathcal{B}_i^{\Lambda\lambda F}(t) = \frac{d_\Lambda}{g_{O_h^D}} \sum_{R \in O_h^D} \Gamma_{\lambda\lambda}^{(\Lambda)}(R) U_R B_i^F(t) U_R^\dagger, \quad (4.5)$$

where  $O_h^D$  is the double group of  $O_h$ ,  $R$  denotes an element of  $O_h^D$ ,  $g_{O_h^D}$  is the number of elements in  $O_h^D$ , and  $d_\Lambda$  is the dimension of the  $\Lambda$  irreducible representation. Projections onto both the single-valued and double-valued irreps of  $O_h$  require using the double group  $O_h^D$  in Eq. (4.5). Given  $M_B$

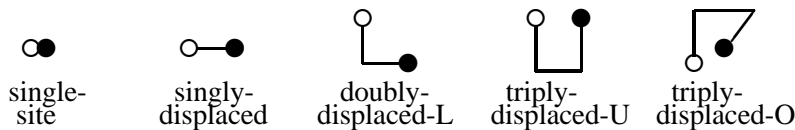


**Figure 8:** The spatial arrangements of the quark-antiquark meson operators. In the illustrations, the smeared quarks fields are depicted by solid circles, each hollow circle indicates a smeared “barred” antiquark field, and the solid line segments indicate covariant displacements.

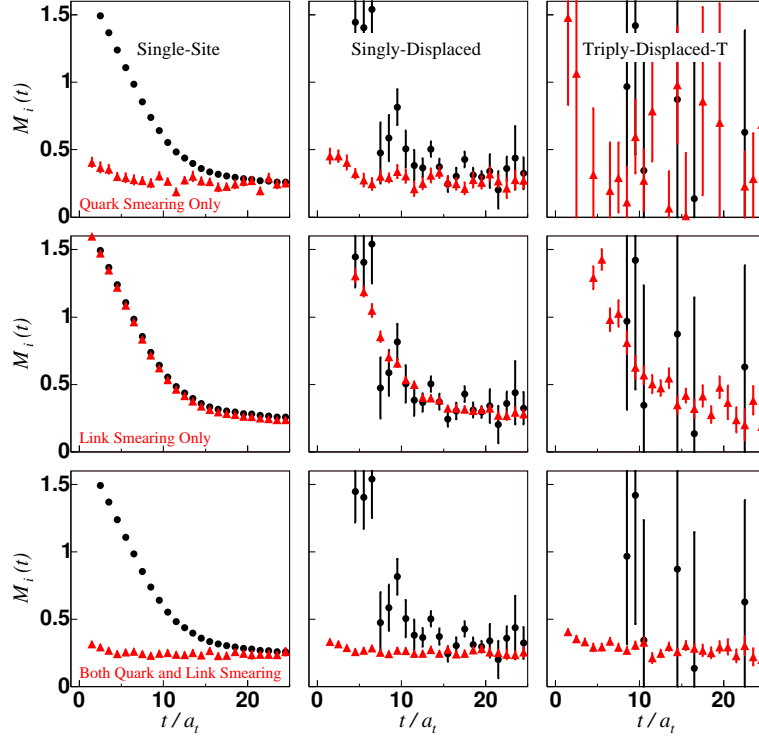


**Figure 9:** Effective masses  $M(t)$  for unsmeared (black circles) and smeared (red triangles) operators  $O_{SS}$ ,  $O_{SD}$ ,  $O_{TDT}$ , which are representative single-site, singly-displaced, and triply-displaced-T nucleon operators, respectively. Top row: only quark-field smearing  $n_\sigma = 32$ ,  $\sigma_s = 4.0$  is used. Middle row: only link-variable smearing  $n_\rho = 16$ ,  $n_\rho\rho = 2.5$  is applied. Bottom row: both quark and link smearing  $n_\sigma = 32$ ,  $\sigma_s = 4.0$ ,  $n_\rho = 16$ ,  $n_\rho\rho = 2.5$  are used, dramatically improving the signal for all three operators. Results are based on 50 quenched configurations on a  $12^3 \times 48$  anisotropic lattice using the Wilson action with  $a_s \sim 0.1$  fm,  $a_s/a_t \sim 3.0$ .

elemental  $B_i^F$  operators, many of the projections in Eq. (4.5) vanish or lead to linearly-dependent operators, so one must then choose suitable linear combinations of the projected operators to obtain a final set of independent baryon operators. Thus, in each symmetry channel, one ends up with a set of  $r$  operators given in terms of a linear superposition of the  $M_B$  elemental operators. The different spatial configurations (see Fig. 7 for the baryon configurations and Fig. 8 for the meson configurations) yield operators which effectively build up the necessary orbital and radial structures of the hadron excitations. The design of these operators is such that a large number of them can be evaluated very efficiently, and components in their construction can be used for both meson, baryon, and multi-hadron computations.

Finding appropriate smearing parameters is a first crucial part of any hadron spectrum calculation. Fig. 9 demonstrates that *both* quark-field and link-field smearing are needed in order for spatially-extended baryon operators to be useful[15]. It is important to use the smeared links when smearing the quark field. Link smearing dramatically reduces the statistical errors in the correlators of the displaced operators, while quark-field smearing dramatically reduces the excited-state contamination.

The above approach to designing hadron and multi-hadron interpolating fields leads to a very

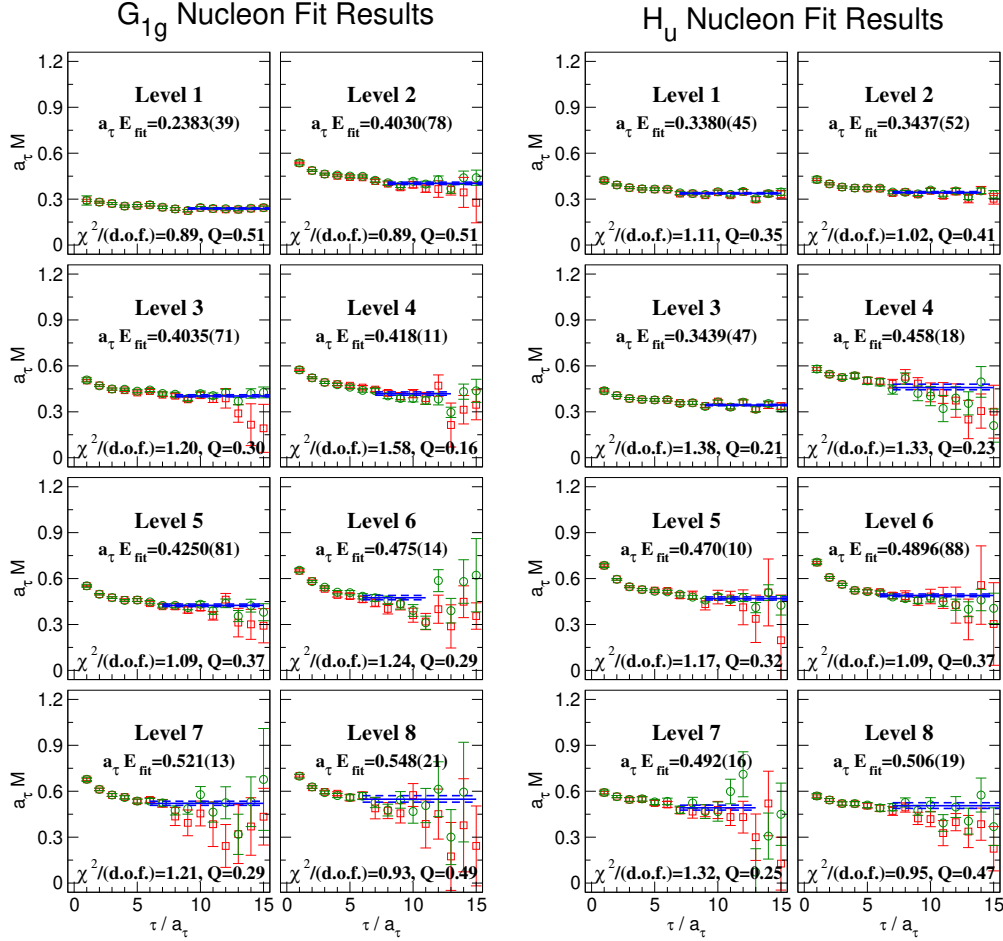


**Figure 10:** Effective masses for the lowest eight levels in the  $G_{1g}$  channel (left) and  $H_u$  channel (right). The green circles are fixed-coefficient effective masses, whereas the red squares are the principal effective masses. Fit values are shown by the blue lines. Results are based on 200 quenched configurations on a  $12^3 \times 48$  anisotropic lattice using the Wilson gauge and quark actions with  $a_s \sim 0.1$  fm,  $a_s/a_t \sim 3.0$  and  $m_\pi \sim 700$  MeV.

large number of operators. It is not feasible to do spectrum computations using all of the operators so designed; for example, in the  $G_{1g}$  symmetry channel for nucleons, the above procedure leads to 179 operators. It is necessary to *prune* down the number of operators. Six months of exploratory testing and trials led to the following guideline: noise is the enemy, so a procedure that keeps a variety of operators while minimizing the effects of noise works best. Some operators are intrinsically noisy and must be removed. In addition, a set of operators, each with little intrinsic noise, can allow noise to creep in if they are not sufficiently independent of one another.

In Ref. [7], the following procedure is advocated. (1) First, remove operators with excessive intrinsic noise. This can be done by examining the diagonal elements of the correlation matrix and discarding those operators whose self-correlators have relative errors above some threshold for a range of temporal separations. Of course, this requires a low-statistics Monte Carlo computation on a reasonably small lattice. (2) Second, prune within operator types (single-site, singly-displaced,

etc.) based on the condition number of the submatrices

$$\hat{C}_{ij}(t) = \frac{C_{ij}(t)}{\sqrt{C_{ii}(t)C_{jj}(t)}}, \quad t = a_t.$$

The condition number is taken to be the ratio of the largest eigenvalue over the smallest eigenvalue. A value near unity is ideal. For each operator type, the set of about six operators which yields the lowest condition number of the above submatrix is retained. (3) Lastly, prune across all operator types based again on the condition number of the remaining submatrix as defined above. In this last step, the goal is to choose about 16 operators, keeping two or three of each type, such that a condition number reasonably close to unity is obtained. As long as a good variety of operators is retained, the resulting spectrum seems to be fairly independent of the exact choice of operators at this stage. Eigenvectors from a variational study of the operators can also be used to fine tune the choice of operators.

Calculations in Ref. [7] using about 16 operators in all irreps for the nucleon channel on only 200 configurations were very successful. The extraction of 8 energy levels in each irrep was possible, which was a major milestone achieved. A determination of the hadron spectrum requires the ability to extract several excited energy levels, and up until that time, it was not known whether or not extracting more than one or two levels would be possible. Fig. 10 shows the signal quality in the  $G_{1g}$  and  $H_u$  irreps for the nucleon excitations from that first calculation. Similar calculations for the  $\Delta$  resonance spectra have also been achieved[16, 17]. Comparison of these results with experiment is not justified since the quenched approximation was used, an unphysically large  $u, d$  quark mass was used, and the lattice volume is too small.

It is my strong opinion that the use of correlation matrices is the best way to extract excited-state energies reliably. However, there are efforts to deduce information about excited states from single correlation functions. Bayesian statistics have been used[18, 19], as well as maximum entropy methods[20, 21]. A novel evolutionary fitting method has been proposed[22], and a new method based on statistical concepts which relies heavily on simulation techniques was presented at this conference[23].

## 5. Stochastic estimates of many-to-many quark propagators with source dilution variance reduction

To study a particular eigenstate of interest, all eigenstates lying below that state must first be extracted, and as the pion gets lighter in lattice QCD simulations, more and more multi-hadron states will lie below the excited resonances. Consider a baryon at rest. An appropriate quantum operator for a baryon at rest typically has the form

$$B(\mathbf{p} = 0, t) = \frac{1}{V} \sum_{\mathbf{r}} \varphi_B(\mathbf{r}, t), \quad (5.1)$$

where  $V$  is the volume of the lattice and  $\varphi_B(\mathbf{r}, t)$  is an appropriate localized interpolating field. In the above equation, the summation over spatial lattices makes the operator translationally invariant, producing a zero momentum state. A baryon correlator, thus, has a double summation over spatial

sites:

$$\langle 0|B(\mathbf{p}=0,t)\bar{B}(\mathbf{p}=0,0)|0\rangle = \frac{1}{V^2} \sum_{\mathbf{x},\mathbf{y}} \langle 0|\varphi_B(\mathbf{x},t)\bar{\varphi}_B(\mathbf{y},0)|0\rangle. \quad (5.2)$$

Evaluating the above correlator requires computing the  $\mathbf{y} \rightarrow \mathbf{x}$  element of the quark propagators. In other words, the quark propagators from all spatial sites  $\mathbf{y}$  on time slice  $t=0$  to all spatial sites  $\mathbf{x}$  on later time slice  $t>0$  must be known. Computing all such elements of the propagators exactly is not possible (except on very small lattices). In the example above, this problem can be circumvented by appealing to translational invariance to limit the summation over the source site to a single site:

$$\langle 0|B(\mathbf{p}=0,t)\bar{B}(\mathbf{p}=0,0)|0\rangle = \frac{1}{V} \sum_{\mathbf{x}} \langle 0|\varphi_B(\mathbf{x},t)\bar{\varphi}_B(\mathbf{0},0)|0\rangle. \quad (5.3)$$

However, a *good* baryon-meson operator of total zero momentum typically has the form

$$B(\mathbf{p},t)M(-\mathbf{p},t) = \frac{1}{V^2} \sum_{\mathbf{x},\mathbf{y}} \varphi_B(\mathbf{x},t)\varphi_M(\mathbf{y},t)e^{i\mathbf{p}\cdot(\mathbf{x}-\mathbf{y})}, \quad (5.4)$$

where  $\varphi_M(\mathbf{y},t)$  is a localized interpolating field for a meson. In the evaluation of the temporal correlations of such a multi-hadron operator, it is not possible to completely remove all summations over the source site. Hence, the need for estimates of the quark propagators from all spatial sites on a time slice to all spatial sites on another time slice cannot be sidestepped. Ultimately, some correlators will involve disconnected diagrams which necessarily involve all-to-all quark propagators. Hence, all-to-all (or many-to-many) quark propagators are becoming mandatory, and some way of stochastically estimating them is needed.

Random noise vectors  $\eta$  whose expectations satisfy  $E(\eta_i) = 0$  and  $E(\eta_i\eta_j^*) = \delta_{ij}$  are useful for stochastically estimating the inverse of a large matrix  $M$  as follows. Assume that for each of  $N_R$  noise vectors, we can solve the following linear system of equations:  $MX^{(r)} = \eta^{(r)}$  for  $X^{(r)}$ . Then  $X^{(r)} = M^{-1}\eta^{(r)}$ , and

$$E(X_i\eta_j^*) = E\left(\sum_k M_{ik}^{-1}\eta_k\eta_j^*\right) = \sum_k M_{ik}^{-1}E(\eta_k\eta_j^*) = \sum_k M_{ik}^{-1}\delta_{kj} = M_{ij}^{-1}. \quad (5.5)$$

The expectation value on the left-hand can be approximated using the Monte Carlo method. Hence, a Monte Carlo estimate of  $M_{ij}^{-1}$  is given by

$$M_{ij}^{-1} \approx \lim_{N_R \rightarrow \infty} \frac{1}{N_R} \sum_{r=1}^{N_R} X_i^{(r)} \eta_j^{(r)*}, \quad \text{where } MX^{(r)} = \eta^{(r)}. \quad (5.6)$$

Unfortunately, this equation usually produces stochastic estimates with variances which are much too large to be useful.

Progress is only possible if stochastic estimates of the quark propagators with reduced variances can be made. Techniques of *diluting* the noise vectors have been developed which accomplish such a variance reduction[24, 25, 26, 27, 28, 29]. A given dilution scheme can be viewed as the application of a complete set of projection operators. To see how dilution works, consider a general  $N \times N$  matrix  $M$  having matrix elements  $M_{ij}$ . Define some complete set of  $N \times N$  projection matrices  $P^{(a)}$  which satisfy

$$P^{(a)}P^{(b)} = \delta^{ab}P^{(a)}, \quad \sum_a P^{(a)} = 1, \quad P^{(a)\dagger} = P^{(a)}. \quad (5.7)$$

Then observe that

$$\begin{aligned} M_{ij}^{-1} &= M_{ik}^{-1} \delta_{kj} = \sum_a M_{ik}^{-1} P_{kj}^{(a)} = \sum_a M_{ik}^{-1} P_{kk'}^{(a)} P_{k'j}^{(a)} = \sum_a M_{ik}^{-1} P_{kk'}^{(a)} \delta_{k'j'} P_{j'j}^{(a)} \\ &= \sum_a M_{ik}^{-1} P_{kk'}^{(a)} E(\eta_{k'} \eta_{j'}^*) P_{j'j}^{(a)} = \sum_a M_{ik}^{-1} E\left(P_{kk'}^{(a)} \eta_{k'} \eta_{j'}^* P_{j'j}^{(a)}\right). \end{aligned} \quad (5.8)$$

Define

$$\eta_k^{[a]} = P_{kk'}^{(a)} \eta_{k'}, \quad \eta_j^{[a]*} = \eta_{j'}^* P_{j'j}^{(a)} = P_{j'j}^{(a)*} \eta_{j'}^* \quad (5.9)$$

and further define  $X^{[a]}$  as the solution of

$$M_{ik} X_k^{[a]} = \eta_i^{[a]}, \quad (5.10)$$

then we have

$$M_{ij}^{-1} = \sum_a M_{ik}^{-1} E(\eta_k^{[a]} \eta_j^{[a]*}) = \sum_a E(X_i^{[a]} \eta_j^{[a]*}). \quad (5.11)$$

Although the expected value of  $\sum_a \eta_k^{[a]} \eta_j^{[a]*}$  is the same as  $\eta_k \eta_j^*$ , the *variance* of  $\sum_a \eta_k^{[a]} \eta_j^{[a]*}$  is significantly smaller than that of  $\eta_k \eta_j^*$ . For both  $Z_4$  and  $U(1)$  noise, we have

$$\text{Var}(\text{Re}(\eta_i \eta_j^*)) = \text{Var}(\text{Im}(\eta_i \eta_j^*)) = \frac{1}{2}(1 - \delta_{ij}).$$

Although the variance is zero for  $i = j$ , there is a significant variance for all  $i \neq j$ . The dilution projections ensure *exact zeros* for many of the off-diagonal elements, instead of values that are only statistically zero. In other words, many of the  $i \neq j$  elements become exactly zero.

Of course, the effectiveness of the variance reduction depends on the projectors chosen. A particularly important dilution scheme for measuring temporal correlations in hadronic quantities is “time dilution” where the noise vector is broken up into pieces which only have support on a single time slice:

$$P_{\alpha\alpha';\beta\beta'}^{(B)}(\mathbf{x}, t; \mathbf{y}, t') = \delta_{ab} \delta_{\alpha\beta} \delta_{\mathbf{xy}} \delta_{Bt} \delta_{Bt'}, \quad B = 0, 1, \dots, N_t - 1, \quad (\text{time dilution}), \quad (5.12)$$

where  $N_t$  is the number of time slices on the lattice,  $a, b$  are color indices, and  $\alpha, \beta$  are spin indices. Spin and color dilution are two other easy-to-implement schemes:

$$P_{\alpha\alpha';\beta\beta'}^{(B)}(\mathbf{x}, t; \mathbf{y}, t') = \delta_{ab} \delta_{B\alpha} \delta_{B\beta} \delta_{\mathbf{xy}} \delta_{t't'}, \quad B = 0, 1, 2, 3, \quad (\text{spin dilution}), \quad (5.13)$$

$$P_{\alpha\alpha';\beta\beta'}^{(B)}(\mathbf{x}, t; \mathbf{y}, t') = \delta_{Ba} \delta_{Bb} \delta_{\alpha\beta} \delta_{\mathbf{xy}} \delta_{t't'}, \quad B = 0, 1, 2, \quad (\text{color dilution}). \quad (5.14)$$

Various spatial dilution schemes are possible, too. For example, even-odd dilutions are simple to implement. The above dilution projectors can also be combined to make hybrid schemes.

Before presenting tests of these different dilution schemes, an important remark about the use of stochastic quark propagators should be mentioned. The use of Eq. (5.11) to approximate quark propagators leads to a very desirable source-sink factorization. Consider a baryon correlator of the form

$$C_{\bar{l}l} = c_{ijk}^{(l)} c_{ijk}^{(\bar{l})*} Q_{\bar{i}\bar{i}}^{(A)} Q_{jj}^{(B)} Q_{\bar{k}\bar{k}}^{(C)}, \quad (5.15)$$

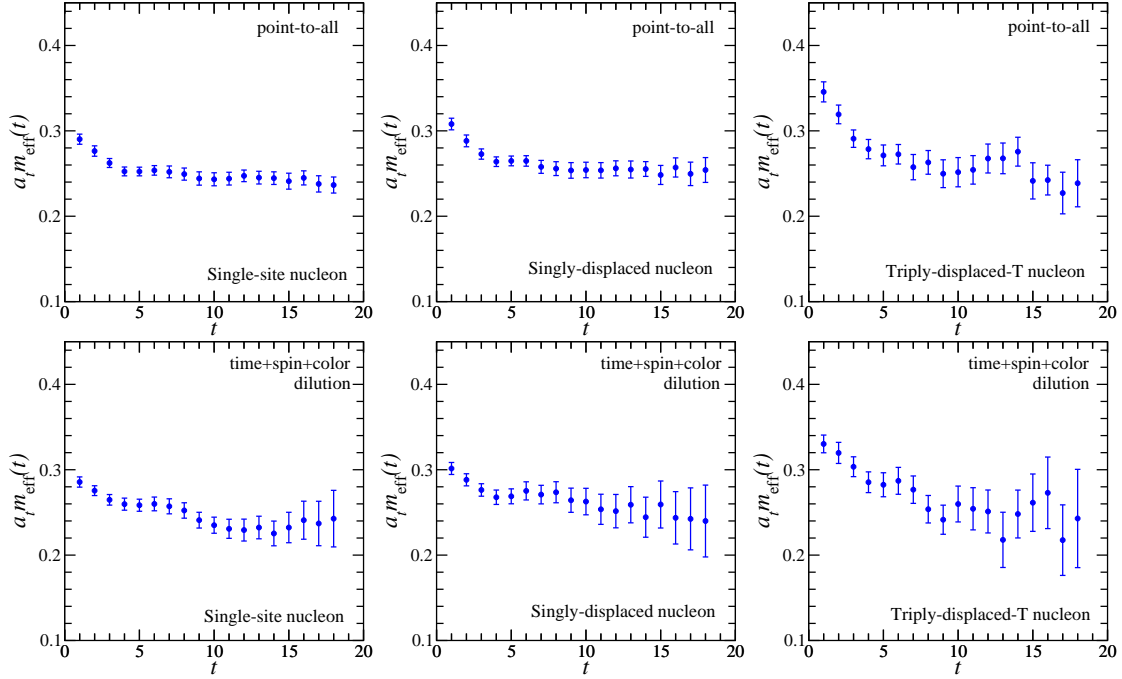


**Figure 11:** (Upper row) Effective masses for a single-site (left), singly-displaced (middle), and triply-displaced-T (right) nucleon operator using quark propagators evaluated with the standard point-to-all method. (Lower row) The effective masses for the same nucleon operators but using stochastic quark propagators with time+spin+color dilution. Without dilutions, the errors in these effective masses would be orders of magnitude larger. An effective mass defined using a time separation  $3a_t$  is used in these plots. These results used 100 quenched configurations on an anisotropic  $12^3 \times 48$  lattice with a Wilson fermion and gauge action.

where  $Q^{(A)}$  denotes a quark propagator of flavor  $A$  and all other quark indices have been combined into a single index  $i$  or  $j$ , and so on. Stochastic estimates of this correlator using Eq. (5.11) lead to the form

$$C_{\bar{l}l} = \frac{1}{N_R} \sum_r \sum_{d_A d_B d_C} c_{ijk}^{(l)} c_{ijk}^{(\bar{l})*} \left( \varphi_i^{(Ar)[d_A]} \eta_i^{(Ar)[d_A]*} \right) \left( \varphi_j^{(Br)[d_B]} \eta_j^{(Br)[d_B]*} \right) \left( \varphi_k^{(Cr)[d_C]} \eta_k^{(Cr)[d_C]*} \right), \quad (5.16)$$

where  $r$  labels the noise vectors,  $d_A, d_B, d_C$  are the dilution indices,  $\eta$  are the noise vectors, and  $\varphi$  are the solution vectors. If one defines

$$\Gamma_l^{(r)[d_A d_B d_C]} = c_{ijk}^{(l)} \varphi_i^{(Ar)[d_A]} \varphi_j^{(Br)[d_B]} \varphi_k^{(Cr)[d_C]}, \quad (5.17)$$

$$\Omega_l^{(r)[d_A d_B d_C]} = c_{ijk}^{(l)} \eta_i^{(Ar)[d_A]} \eta_j^{(Br)[d_B]} \eta_k^{(Cr)[d_C]}, \quad (5.18)$$

then the baryon correlator becomes a glorified dot product of the source vector with the sink vector:

$$C_{\bar{l}l} = \frac{1}{N_R} \sum_r \sum_{d_A d_B d_C} \Gamma_l^{(r)[d_A d_B d_C]} \Omega_l^{(r)[d_A d_B d_C]*}. \quad (5.19)$$

The source and sink vectors in Eqs. (5.17) and (5.18) can be separately evaluated for a variety of operators, and the dot product applied afterwards to evaluate the matrix of correlation functions.

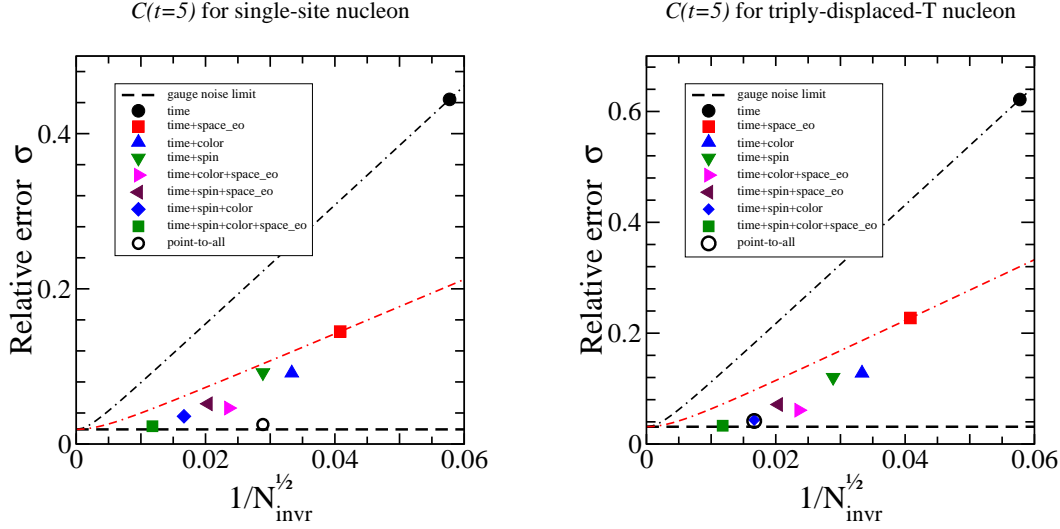


**Figure 12:** (Left) The relative errors in the correlation function of a single-site nucleon operator for temporal separation  $t = 5a_t$  evaluated using stochastically-estimated quark propagators with different dilution schemes against  $1/N_{\text{inv}}^{1/2}$ , where  $N_{\text{inv}}$  is the number of Dirac matrix inversions required. The open circle shows the point-to-all error, and the horizontal dashed line shows the gauge-noise limit. The black (red) dashed-dotted line shows the decrease in error expected by simply increasing the number of noise vectors, starting from the time (time + even/odd-space) dilution point. (Right) Same as the left plot, except for a triply-displaced-T nucleon operator. These results used 100 quenched configurations on an anisotropic  $12^3 \times 48$  lattice with a Wilson fermion and gauge action.

Different  $ABC$  permutations of the noise vectors must be stored in order to accommodate all needed Wick contractions. The use of stochastic all-to-all quark propagators has led to an enormous simplification of the effort required to compute the hadron correlation matrices through this source-sink factorization. Another advantage of this approach is the fact that, given suitable non-zero momenta, these same baryon and meson operators can be combined later to make multi-hadron operators.

The effectiveness of stochastically-estimated all-to-all quark propagators using diluted noise vectors is demonstrated in Fig. 11. This figure compares the effective masses for a single-site, singly-displaced, and triply-displaced-T nucleon operator using quark propagators evaluated with the conventional point-to-all method (top row) and with the all-to-all stochastic method including time+spin+color dilutions (bottom row). The fact that these effective masses have comparable errors indicates that the stochastic method with suitable dilutions has not introduced any appreciable noise into the final mass extractions.

A comparison of different dilution schemes has been presented at this conference[30]. Fig. 12 shows the relative errors in the correlation functions of a single-site and a triply-displaced-T nucleon operator for temporal separation  $t = 5a_t$  evaluated using stochastically-estimated quark propagators with different dilution schemes against  $1/N_{\text{inv}}^{1/2}$ , where  $N_{\text{inv}}$  is the number of matrix inversions required. These results were obtained using 100 quenched configurations on an anisotropic  $12^3 \times 48$  lattice with a Wilson fermion and gauge action. The open circles show the point-to-all errors, and the horizontal dashed lines show the gauge-noise limits. The black (red) dashed-dotted



lines show the decrease in error expected by simply increasing the number of noise vectors, starting from the time (time + even/odd-space) dilution points. These computations are dominated by the inversions of the Dirac matrix, so using the number of matrix inversions  $N_{\text{inv}}$  to compare computational efforts is reasonably fair. The advantage in using increased dilutions compared to an increased number of noise vectors with only time dilution is evident in the plots. However, this advantage quickly diminishes after time + even/odd-space dilution, or time+color, or time+spin dilution. Note that time+spin+color+even/odd-space dilution yields an error comparable with the gauge-noise limit using only a single noise vector! First results for multi-hadron operators were also presented at this conference[31].

These encouraging results demonstrate that the inclusion of good multi-hadron operators will certainly be possible using stochastic all-to-all quark propagators with diluted-source variance reduction. In fact, just before this conference, the authors of Ref. [9] began exploring a new method that might allow nearly-exact determinations of many-to-many quark propagators without introducing any noise vectors at all. The method exploits a novel, cleverly-devised choice of quark-field smearing to facilitate the nearly-exact computations. Details and tests of this method should appear very soon.

## 6. Summary and outlook

This talk discussed the key issues and challenges in exploring excited hadrons in lattice QCD. The importance of multi-hadron operators and the need for all-to-all quark propagators were emphasized. The challenge of dealing with unstable states (resonances) in a box was outlined, and the technology associated with extracting excited stationary-state energies, including operator design and field smearing, was detailed. Efforts in variance reduction of stochastically-estimated all-to-all quark propagators using source dilutions were described, and results on excited hadrons which appeared during the last year were summarized.

Given the major experimental efforts to map out the QCD resonance spectrum, such as Hall B and the proposed Hall D at Jefferson Lab, ELSA associated with the University of Bonn, COMPASS at CERN, PANDA at GSI, and BESIII in Beijing, there is a great need for *ab initio* determinations of such states in lattice QCD. The exploration of excited hadrons in lattice QCD is well underway.

This work was supported by the National Science Foundation through awards PHY 0653315 and PHY 0510020.

## References

- [1] A. Csoto, B. Gyarmati, A. Kruppa, K. Pal, N. Moiseyev, Phys. Rev. A **41**, 3469 (1990).
- [2] C. McNeile and C. Michael, Phys. Lett. **B556**, 177 (2003).
- [3] B. DeWitt, Phys. Rev. **103**, 1565 (1956).
- [4] M. Luscher, Nucl. Phys. **B364**, 237 (1991).
- [5] G. Schierholz, these proceedings.
- [6] V. Bernard, M. Lage, U.G. Meissner, A. Rusetsky, JHEP **0808**, 024 (2008).

- [7] A. Lichtl, Ph.D. thesis, Carnegie Mellon University [hep-lat/0609019].
- [8] S. Basak, R. Edwards, G. Fleming, K. Juge, A. Lichtl, C. Morningstar, D. Richards, I. Sato, S. Wallace, Phys. Rev. D **76**, 074504 (2007).
- [9] J. Bulava, J. Foley, C. Morningstar, J. Dudek, R. Edwards, B. Joo, H.W. Lin, D. Richards, E. Engelson, S. Wallace, A. Lichtl, N. Mathur, in preparation (also, see these proceedings).
- [10] C. Gattringer, L. Glozman, C. Lang, D. Mohler, S. Prelovsek, Phys. Rev. D **78**, 034501 (2008).
- [11] S. Prelovsek, these proceedings.
- [12] M. Lüscher and U. Wolff, Nucl. Phys. **B339**, 222 (1990).
- [13] S. Basak, R.G. Edwards, G.T. Fleming, U.M. Heller, C. Morningstar, D. Richards, I. Sato, S. Wallace, Phys. Rev. D **72**, 094506 (2005).
- [14] C. Morningstar and M. Peardon, Phys. Rev. D **69**, 054501 (2004).
- [15] A. Lichtl, C. Morningstar, S. Basak, I. Sato, S. Wallace, R. Edwards, D. Richards, G. Fleming, U. Heller, PoS LAT2005:076 (2006).
- [16] J. Bulava, R. Edwards, G. Fleming, K.J. Juge, A. Lichtl, N. Mathur, C. Morningstar, D. Richards, S.J. Wallace, AIP Conf. Proc. **947**, 77 (2007) (arXiv:0708.2072 [hep-lat]).
- [17] J. Bulava, R. Edwards, G. Fleming, K.J. Juge, A. Lichtl, N. Mathur, C. Morningstar, D. Richards, S.J. Wallace, AIP Conf. Proc. **947**, 137 (2007) (arXiv:0708.2145 [hep-lat]).
- [18] G.P. Lepage, B. Clark, C. Davies, K. Hornbostel, P. Mackenzie, C. Morningstar, H. Trotter, Nucl. Phys. B (Proc. Suppl.) **106**, 12 (2002) [hep-lat/0110175].
- [19] C. Morningstar, Nucl. Phys. (Proc. Suppl.) **109A**, 185 (2002) [hep-lat/0112023].
- [20] K. Sasaki, S. Sasaki, T. Hatsuda, Phys. Lett. **B623**, 208 (2005).
- [21] M. Cook, H.R. Fiebig, PoS LAT2006:172,2006.
- [22] G. von Hippel, R. Lewis, R. Petry, Comput. Phys. Commun. **178**, 713 (2008).
- [23] C. Alexandrou, C.N. Papanicolas, E. Stiliaris, arXiv:0810.3982 [hep-lat] (2008).
- [24] J. Foley, K.J. Juge, A. O’Cais, M. Peardon, S. Ryan, J.I. Skullerud, Comput. Phys. Commun. **172**, 145 (2005).
- [25] S. Bernardson, P. McCarty, C. Thron, Comput. Phys. Commun. **78**, 256 (1993).
- [26] W. Wilcox, in *Lecture Notes in Computational Science and Engineering*, Vol. 15, pp. 127-141 (2000) [hep-lat/9911013].
- [27] W. Wilcox, B. Lindsay, Nucl. Phys. B (Proc. Suppl.) **63**, 973 (1998) [hep-lat/9708028].
- [28] H. Neff, N. Eicker, T. Lippert, J. Negele, K. Schilling, Phys. Rev. D **64**, 114509 (2001).
- [29] S. Collins, G. Bali, A. Schafer, PoS LAT2007:141 (2007) (arXiv:0709.3217 [hep-lat]).
- [30] J. Bulava, R. Edwards, C. Morningstar, these proceedings (arXiv:0810.1469 [hep-lat]).
- [31] J. Bulava, R. Edwards, K.J. Juge, C.J. Morningstar, M.J. Peardon, these proceedings (arXiv:0810.0730 [hep-lat]).